Lateral resolution and potential sensitivity in Kelvin probe force microscopy: Towards understanding of the sub-nanometer resolution

F. Krok,* K. Sajewicz, J. Konior, M. Goryl, P. Piatkowski, and M. Szymonski
Research Centre for Nanometer-Scale Science and Advanced Materials (NANOSAM), Faculty of Physics, Astronomy and Applied Computer Science, Jagiellonian University, Reymonta 4, 30-059 Krakow, Poland
(Received 20 December 2007; revised manuscript received 5 May 2008; published 18 June 2008)

We report on high-resolution potential imaging of heterogeneous surfaces by means of Kelvin probe force microscopy, working in frequency modulation mode (FM-KPFM), performed in ultrahigh vacuum. To study the limits of potential and lateral resolutions in FM-KPFM, we have investigated clean surface of compound semiconductor InSb(001) and the same surface with some submonolayer coverages of KBr and Au. It was found that long- and short-range bias-dependent interactions, acting between the tip and the surface, could be detected and that both interactions contribute to the measured contact potential difference (CPD) signal. On the one hand, when only the long-range electrostatic interactions between the tip and the surface are active, the CPD map provides the distribution of the local surface potential on the imaged sample with the lateral resolution and the correctness of the measured values depending on the measurement conditions. For this case, the experimental findings were compared with the predictions of theoretical calculations based on a realistic model for the cantilever-sample geometry. On the other hand, when the short-range and bias-dependent interactions are detected, FM-KPFM provides even the sub-nanometer contrast in the CPD signal. In this situation, however, the measured CPD signal is not related to the sample surface potential but reflects the properties of the front tip atom-surface atom interactions.

DOI: 10.1103/PhysRevB.77.235427 PACS number(s): 68.37.Ps, 81.05.Ea, 68.55.−a, 73.40.Cg

I. INTRODUCTION

Design and production of nanoscale structures is one of the primary tasks in current research related to nanotechnology. Therefore, there is a requirement for developing a nondestructive, diagnostic tool that could probe a variety of surface related properties down to a nanometer scale range. The Kelvin probe force microscopy (KPFM) technique,[1,2] based on dynamic force microscopy (DFM) principles, gives both topography and potential distribution of the sample together with a high spatial resolution. In DFM, the vibrating tip moves over the surface at distances where the tip-surface forces are attractive. One of the interactions acting between the tip and the surface is the electrostatic one due to the difference between the tip and the sample work functions (Φ). In general, if the electrons are allowed to flow between two different conducting materials (in this case, the tip and the surface are connected by an effective wire), there will be a contact potential between them as the electrons must pay some energy to travel from the material with the smaller work function to the material with the higher one. The difference of the work functions defines the contact potential difference (CPD) between the tip and the sample, $V_{CPD}=(\Phi_{tip}-\Phi_{sample})/e$. By applying an external bias voltage and, thus, compensating V_{CPD}, KPFM technique effectively enables to remove the electrostatic interaction from the total tip-sample interactions, and that allows for both topography and contact potential images of the sample to be acquired simultaneously. It is assumed that the presence of the tip in close proximity to the sample surface does not change its electronic properties as long as the chemical composition of the tip apex remains unchanged. As a consequence, the values of sample work function provided with KPFM are the same as those measured with other spectroscopic techniques, for example, with ultraviolet photoemission spectroscopy (UPS).[3]

Among many applications, KPFM technique has been applied for work function mapping,[4] evaluation of doping concentration in semiconductors,[5] and for determining a local work function distribution in quantum dots.[6] For imaging of heterogeneous surfaces, the KPFM has already shown its advantage over the standard DFM microscopy as due to the compensation of the electrostatic forces, the height profiles obtained in the topography images are more reliable.[7] Moreover, for some heterogeneous surfaces, by using KPFM, not only true topography is recorded but also the chemical contrast can be obtained.[8]

From many crucial aspects concerning KPFM technique, the limits of potential sensitivity and lateral resolution are particularly important. Recently, lateral resolution on the atomic scale in the CPD signal has been reported[9,10] but its origin is still poorly understood, mainly due to the long-range nature of electrostatic forces. A big effort is undertaken, both on the experimental as well as on the theoretical side, to explain the observed features.

In this work, we present the experimental and theoretical results concerning the lateral resolution of surface potential, measured in ultrahigh vacuum (UHV) FM-KPFM. The measured CPD contrast is then compared with the predictions of a theoretical model that takes into account long-range tip-sample electrostatic interactions. We have also confirmed experimentally the existence of some short-range and bias-dependent tip-surface interactions. A detection of these short-range interactions with KPFM could provide, finally, the CPD contrast with lateral resolution in the range of atomic distances.

The paper is organized as follows. In Sec. II, we describe the experimental system used in the present study. In Secs.

III A and III B, we discuss the issue of CPD signal accuracy on the example of FM-KPFM imaging of KBr/InSb(001). In Sec. III C, we present the results of FM-KPFM imaging of bare InSb(001) surface with sub-nanometer resolution. In Secs. III D and III E, on the example of FM-KPFM imaging of Au/InSb(001) system, we provide experimental evidence of detection with FM-KPFM of short-range and bias-dependent interactions, acting between the tip and the surface. Based on the experimental findings and theoretical analyses in Sec. IV, we discuss the origin of interactions, contributing to the measured CPD signal. Finally, Sec. V summarizes the paper.

II. EXPERIMENT

The experiments were performed in an interconnected 3-chamber UHV system, allowing for sample preparation, analysis, and SPM imaging under the same UHV environment. The details of the UHV system are given elsewhere.[11] To study the resolution of FM-KPFM, we have used the compound semiconductor InSb(001) as a substrate covered with a submonolayer of KBr and Au. The substrate surface—prepared by a few cycles of Ar^+ beam bombardment ($2\ \mu A/cm^2$ at 700 eV for 30 min) with the subsequent annealing up to 750 K for few hours—are composed of large, atomically flat terraces. The epitaxial growth of KBr film on a clean surface of InSb(001), kept at the temperature of 370 K, was performed using a Knudsen effusion cell, heated to the temperature of 720 K; the deposition rate was equal to 0.8 ML/min, as calibrated with a quartz-crystal microbalance prior to the film growth. The deposition of gold on the semiconductor surfaces was performed with home made, resistively heated ceramic crucible and the deposition rate was 0.1 ML/min. The gold overlayer growth on InSb(001) was performed at two substrate surface temperatures of 400 and 560 K. The pressure in the chamber during the film growth was at the level of low 10^{-10} mbar.

The UHV KPFM microscope is a modified VP2 AFM/STM Park Scientific Instruments device,[8] operating at a pressure of 5×10^{-11} mbar and at room temperature (RT). In the measurements, the topography was acquired using noncontact FM mode with a silicon (boron-doped) piezoresistive cantilevers purchased from Park Scientific Instruments. The tip, prior to the measurement, was cleaned in the UHV conditions by thermal annealing to about 1100 K by passing a current (6 mA for 1 min) through the resistive legs of the cantilever, following the procedure described in Ref. 12. The tip of conical shape with the half opening angle of about 20° has the apex radius of about 20 nm as checked with the high–resolution scanning electron microscope. During the experiments, the frequency shift Δf (detuning) relative to the resonant frequency was set in the range −3 to −110 Hz, and a constant oscillation amplitude A was kept in the range between 20 and 50 nm; scanning rate was 0.2–0.5 scan line per second. For the CPD measurements, the sample was biased with a *dc* voltage plus an *ac* voltage of angular frequency $\omega/2\pi=600$ Hz and amplitude $V_{ac}=300$ mV. The time-dependent tip-sample interaction with an angular frequency ω induces the variation of FM demodulator (Nanosurf "easy-PLL") output (the error signal). This ω component of the error signal is detected through a lock-in amplifier (Stanford Research Systems, SR510), then a feedback loop (Kelvin controller) is used to add a *dc* voltage to the sample in order to compensate the contact potential difference between the tip and the sample. As a result, the acquired *dc* map represents the distribution of the measured sample surface potential.

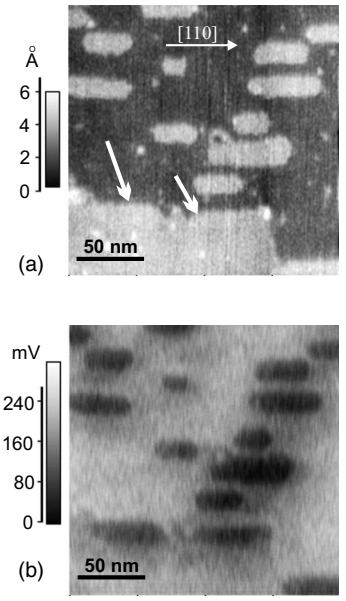

FIG. 1. (a) FM-KPFM topography and (b) ΔCPD images of KBr islands grown on InSb(001) surface ($f_0=111$, 1 kHz, $\Delta f=-17$ Hz). The white arrows indicate the KBr islands, which are topographically not resolved from the substrate terrace.

III. RESULTS

A. FM-KPFM measurements of KBr/InSb(001) system—accuracy of measured CPD signal

A typical topography of KBr islands, grown on InSb(001) surface, is presented in Fig. 1(a). The substrate surface consists of two atomically flat terraces separated by a monoatomic step and the grown KBr islands are visible as the bright features. The islands are of rectangular shape, being elongated along the ⟨110⟩ surface direction. The island shapes indicate that the diffusion of KBr molecules during the film growth is highly anisotropic and this is due to the structure of substrate surface, which is composed of atomic rows along the ⟨110⟩ direction.[13] The KBr molecules aggregate into compact islands of different lateral size but uniform in height (i.e., of monoatomic thickness). The average lateral dimensions of grown islands can be controlled by the amount of deposited material, i.e., the surface coverage. Depending on the nominal surface coverage of KBr, islands as small as a few nm^2 and as large as 100×100 nm^2 can be created with the coverage in the range from 0.2 to 0.7 ML of KBr, respectively. In Fig. 1(b), a contact potential difference image [the ΔCPD (Ref. 14) map] of KBr/InSb(001) surface, acquired simultaneously with topography, is shown. The

dark features on the ΔCPD map correspond to the KBr islands. The map represents the voltage applied to the sample in order to compensate the CPD between the surface and the tip. Thus, a darker contrast on KBr islands (lower voltage) corresponds to a locally decreased work function of the islands, as compared with the substrate.

There is one straightforward observation emerging from Figs. 1(a) and 1(b), which demonstrates the advantage of using KPFM for imaging heterogeneous surfaces. Namely, there are some KBr islands [marked by arrows in Fig. 1(a)] that have grown up attached to the substrate terrace edge and they can be recognized only if the CPD signal is acquired simultaneously with the topography. Figure 1(b) also demonstrates that the CPD signal is not homogeneous across the whole substrate surface area, i.e., the signal gets lowered when measured close to or between the islands. The nonuniformity of the substrate work function points out to the issue of the accuracy of CPD signal measurements.

A wide range of KBr island size, grown on InSb, makes it a model system to study the lateral resolution as well as for checking the accuracy of KPFM contrast. In the following analysis, we assume that the contact potential of KBr islands does not depend on their lateral dimensions at least for two reasons. First, the islands are uniform in their height with no significant rearrangement of the substrate surface under a KBr film.[15] Second, the KBr film is stabilized mostly by Br ions bound to In atoms at the interface.[16] If so, then the associated charge transfer, which is assumed to significantly contribute to the observed change of the work function, should be related to the interacting atoms but not to the size of an island as a whole. Recently, Sasahara *et al.*[17] have shown that considering islands as a perfectly arranged set of electric dipoles with the dipole moment perpendicular to the island surface, the electrostatic potential over the islands should depend on the island size. However, according to their model and for island size studied in the present work, the expected change of electrostatic potential should be in the range of our experimental uncertainties. Because of that, we have not considered the effect.

To determine the relative change of the island work function with respect to the substrate surface work function, we first employed the point Kelvin probe force spectroscopy (KPFS) performed over the substrate surface and some large KBr islands. In the KPFS, the parabolic plots of the detuning versus sample bias voltage were acquired (not shown here) since the electrostatic force is a quadratic function of the bias voltage.[18] The relative difference of the sample bias voltage, corresponding to the parabola maximum, provides the difference in the contact potentials of the surface sites were the spectroscopy is performed. By means of KPFS, we have found that the work function of KBr film (or the KBr/InSb interface) is lower by about 210 meV with respect to the work function of the bare and clean InSb surface.

For studying the limits of the CPD signal accuracy in FM-KPFM measurements, we have analyzed the dependence of ΔCPD, as taken over the KBr islands, on lateral island dimensions. We selected the islands with the length to width ratio not higher than 1.5 and then we assumed the islands to be of equivalent quadratic shape. In Fig. 2, the normalized ΔCPD, as a function of the KBr island size (i.e., the island side length), is shown. It is clear that the measured ΔCPD depends on the size of the islands and the ΔCPD saturates for the island size larger than 100 nm. The value of the saturated ΔCPD in FM-KPFM corresponds to the values measured with point KPFS and indicates that there is no observable tip-induced band bending effect for the system under study, as demonstrated recently by Rosenwaks *et al.*[19] We have found that the observed saturation of the ΔCPD for islands of size around 100 nm is in good agreement with the previously reported lateral resolution of FM-KPFM of 50 nm, obtained by Zerweck *et al.*,[20] when only a single boundary of KCl island grown on Au was imaged. When even smaller KBr islands are imaged, the tip obviously also senses the contact potential of the substrate, and hence, the ΔCPD is significantly reduced. According to the experimental data, when the size of the KBr islands is comparable to the size of the tip apex (i.e., about 20 nm), the CPD signal provides only about 50% of the correct potential value (see Fig. 2).

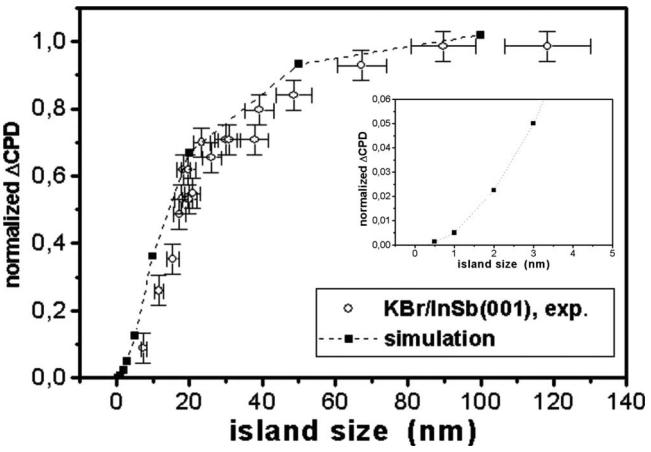

FIG. 2. Measured ΔCPD over the KBr islands versus their size (open circles). The values are normalized (0 mV≡0 and −210 mV≡1) in order to compare with the numerical calculations (solid circles). The calculations were performed for square island of potential $V_{\text{island}}=1$ V surrounded by the infinite plane with potential of 0 V. In the simulations, the tip of radius $r_{\text{tip}}=20$ nm vibrates with the amplitude of $A=40$ nm and the closest tip-surface approach is set to $z_{\text{min}}=1$ nm.

B. Numerical calculation of CPD contrast

There are two effects that may influence the correctness of CPD measurements, which should be considered and they both stem from the long-range nature of electrostatic forces. First, the averaging of the measured CPD due to contribution of whole tip, which is much larger than the island itself. Thus, the region surrounding the island contributes to the measured CPD values. Second, the tip vibrations make the obtained CPD values averaged over the whole tip trajectory.

In order to analyze the effect of experimental conditions on the accuracy of FM-KPFM results, we calculated numerically the correction potential for realistic tip-surface geometry and for a nonuniform potential distribution on the surface. As the first step of the calculation, an electrostatic tip-surface force was evaluated with an efficient method suitable

for an arbitrary surface-potential distribution.[21] The details of the force calculation were given in Ref. 21 and we followed that approach in the correction potential calculation.

For a given tip-plane geometry and an arbitrary plane potential distribution $V_1(x,y)$, the calculated electrostatic tip-surface force is a quadratic function, the tip potential V_0,

$$F_z = \alpha V_0^2 + \beta V_0 + \gamma, \tag{1}$$

with the coefficients α, β, and γ being functions of the tip-surface distance $z_{\min}$. To calculate the frequency shift Δf, we followed the dynamical approach using the integral formula derived by Giessibl,[22]

$$\frac{\Delta f}{f_0} = \frac{-1}{\pi A k}\int_{-1}^{1} F_z[z_{\min} + A(1+u)]\frac{u}{\sqrt{1-u^2}}du$$
$$= \alpha_1 V_0^2 + \beta_1 V_0 + \gamma_1, \tag{2}$$

where the last identity comes from the form of the force [Eq. (1)] so the coefficients α_1, β_2, and γ_1 are calculated by one dimensional integrations, f_0 is the resonance frequency, and A is the vibration amplitude. Then, the correction potential V_{corr} is defined by requiring the frequency shift to be at minimum. Therefore, from Eq. (2), we derive

$$V_{\text{corr}} = -\frac{\beta_1}{2\alpha_1}. \tag{3}$$

We chose a model system in which the tip consists of a cone of length $L_{\text{tip}}=3$ μm, with a half angle $\theta=10°$, and with spherical end segments of radius r_{tip}. The bottom point of the tip has the coordinates $[x_c, y_c, z_{\min}]$; for simplicity, the cantilever is not included in the calculation performed. On the sample surface side, we consider an infinite plane with a square potential island of 1 V, centered at $[x_c, y_c, z=0]$, and of variable size dimension; the rest of the plane has the potential equal to zero.

We have studied the dependence of the calculated CPD contrast on different experimental parameters such as the amplitude of the tip variation A, the closest tip-surface approach $z_{\min}$, and the size of the tip apex, r_{tip} (the detailed results will be presented in a forthcoming paper). In Fig. 2, the calculated results are shown for the experimental value of $A=40$ nm; the other input parameters have the values of $z_{\min}=1$ nm and $r_{\text{tip}}=20$ nm, which were the fit result to experimental results of the ΔCPD dependence on the island size. Taking into account the sensitivity threshold at the level of 5% of the total signal, the calculation shows that the limit of the lateral resolution in FM-KPFM, in the approach presented above, is of 3 nm (see inset of Fig. 2). The predictions are in an agreement with the experimental results where two KBr islands, separated by 4 nm from each other, are distinguished in the CPD map.[23] Our calculations show also that the lateral resolution in the CPD signal can be still improved if the tip with sharper apex can be used.

C. FM-KPFM of InSb(001) surface. Limits of lateral resolutions in CPD signal

Once we have discussed the capability of FM-KPFM to map the true values of the surface potential, the second question arises concerning the observed lateral resolution of the CPD contrast in the sub-nanometer scale. In Fig. 3, a high-resolution image of bare InSb(001) surface topography [Fig. 3(a)] with the corresponding ΔCPD map [Fig. 3(b)] is shown. The surface is composed of atomic rows running along the $\langle 110 \rangle$ crystallographic direction. Based on earlier studies, the presented topography structure image is recognized as the image of the surface indium sublattice,[13] where the dominant indium chains, labeled In1, protrude about 1.2 Å over the rest of the surface. It should be noted here that, according to a model of reconstructed (001) surfaces of AIIIBV semiconductor compounds,[24] the In1 atoms protrude of about 0.9 Å over the neighboring surface atoms. Thus, it is assumed that the imaging of the InSb(01) surface in the constant detuning mode traces the surface with the relative changes of the tip-surface distance over atomic sites of about 0.3 Å.

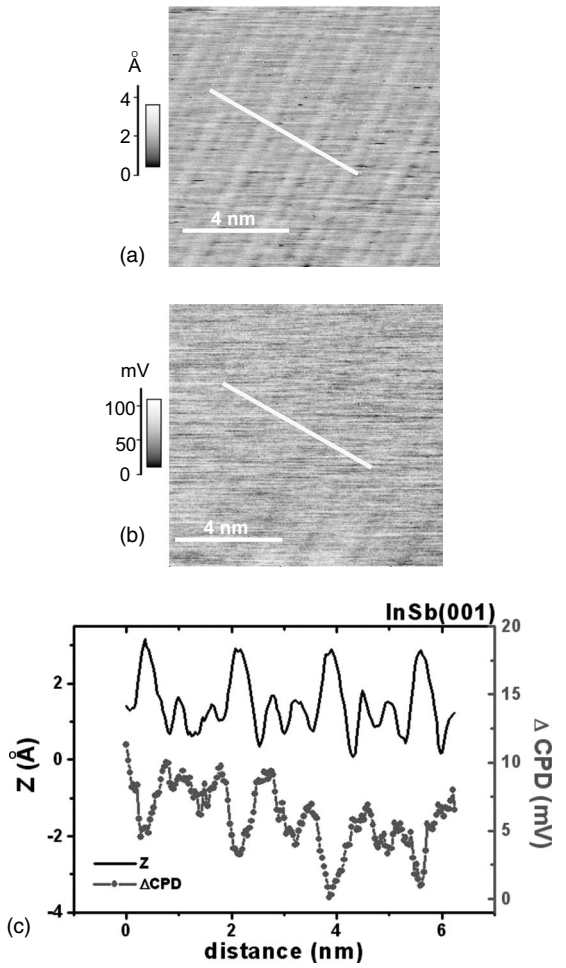

FIG. 3. High resolution (a) FM-KPFM topography and (b) ΔCPD images of InSb(001) surface. (c) Topography (solid line) and ΔCPD (solid circles) profiles along the lines on images (a) and (b). The profiles are averaged over a few lines as shown in (a) and (b). Images acquired with $\Delta f=-112$ Hz and scan rate 0.5 scan line per sec.

In the corresponding ΔCPD map, one can recognize similar structure of dark stripes running parallel to the topographic atomic rows. In Fig. 3(c), topography (solid line) and ΔCPD (solid circles) profiles along the lines in the two 2D

images (a) and (b) are presented. In the ΔCPD signal profile, there are dips of about 5 mV in magnitude, which are out of phase with the topographic features corresponding to the dominant indium atomic chains. This proves that FM-KPFM makes it possible to obtain the modulation of the measured contact potential signal with the lateral resolution on atomic scale level. However, the question appears if the measured modulation in the CPD signal reflects the variation of the work function on the atomic scale level as the meaning of the work function stems from a macroscopic concept. The CPD measurements in KPFM makes use of the concept of minimization of electrostatic tip-surface interactions. Then, because of the long-range nature of these interactions, the measurements would be affected by many tip and sample atoms, as it is shown in the present paper for a KBr/InSb(001) system, both experimentally and theoretically. Thus, the lateral modulation of the CPD signal, visible in the range of distances comparable to the surface atom separations, indicates a presence of some short-range tip-surface interactions, which are probed and compensated with the Kelvin controller. These interactions are bias-dependent and most likely related to the tip front atom and the surface atom underneath. Recently, Arai and Tomitori[25] reported that some specific short-range interactions are bias dependent. Using a silicon tip over Si(111) surface, they have found that the Δf (detuning) deviates from its quadratic dependence on the bias voltage (U_{bias}) when the tip-surface closest separation is lower than about 0.5 nm. They attribute this effect to the appearance of some attractive force due to a quantum-mechanical resonance between the aligned Fermi levels of the surface and the tip. When the curve $\Delta f(U_{\text{bias}})$ deviates from a parabolic one, the global minimum of parabola curve splits into some local minima, which can be found by compensating controller in KPFM, thus providing the CPD signal. However, the obtained voltage cannot be directly related to the contact potential difference between the tip and the surface.

D. FM-KPFM of Au/InSb(001) system

To explore in more details the issue about which interactions are detected by the KPFM, we have performed FM-KPFM imaging of nanostructures formed during a deposition of gold on semiconductor surfaces. In Fig. 4, the topography (part a) and ΔCPD images (part b) of Au grown on InSb(001) are shown, respectively. For the experimental conditions used, gold grows predominantly in a form of rectangular islands with typical height of a few monolayers of Au (about 2.0 nm) and with certain amount of material spread over the substrate surface (i.e., between the islands).[26] From the comparison between the topography and ΔCPD images, it follows that the ΔCPD map provides more details concerning the developed surface topography. Some small features that are difficult to be seen in the topography image, due to a large variation in the image Z direction, are easily recognized with the help of ΔCPD signal. Moreover, almost the same ΔCPD contrast for Au islands and spread material indicates that they are of the same chemical composition. Thus, KPFM is able to give the information about the chemical composition of surface morphology, provided there is some reference

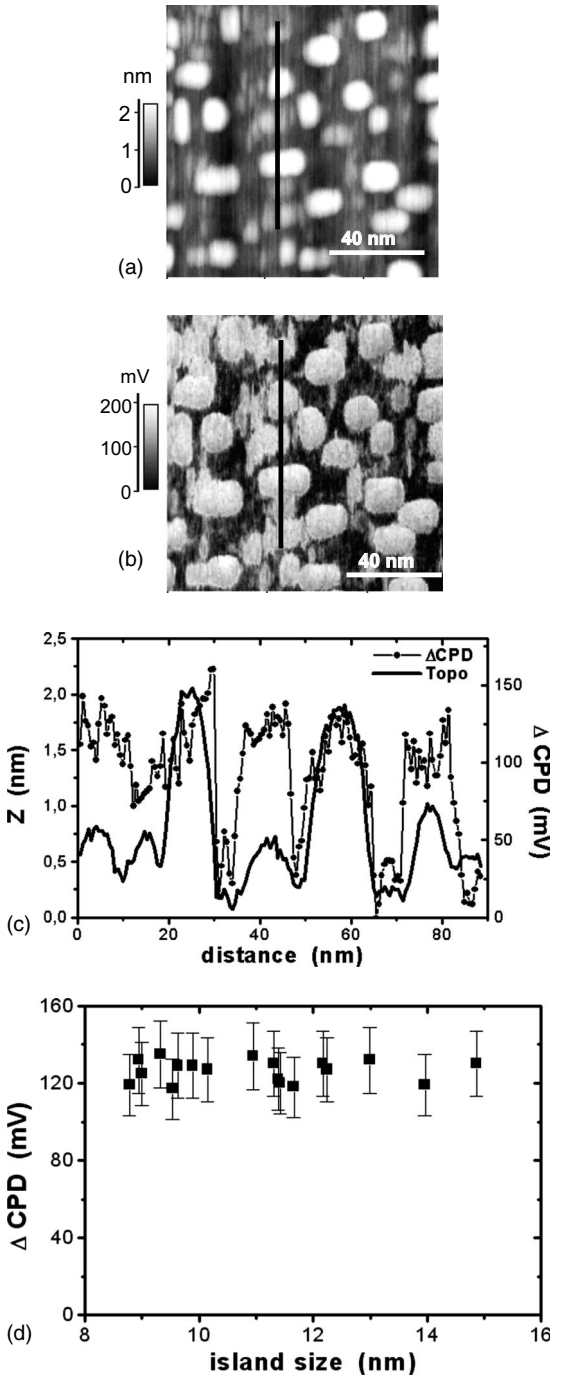

FIG. 4. (a) FM-KPFM topography and corresponding (b) ΔCPD map of 0.2 ML Au grown on InSb(001) surface at 400 K (f_0 =249, 0 kHz, Δf=−6 Hz). (c) Topography (solid line) and ΔCPD (solid circles) profiles taken along the lines in images (a) and (b). (d) Measured ΔCPD versus lateral size of the 2 nm high Au islands.

marker on the imaged surface, i.e., the Au islands in this study. The gold topographic features have higher surface potential in comparison with the substrate surface according to what, in general, is expected due to higher work function of gold with respect to a clean InSb surface. However, despite a large difference in the amount of material constituting both the islands and the features seen between the islands, as well as the difference in their lateral dimensions, both kinds of

structures give almost the same ΔCPD. This is in contrast with the observed dependence of the work function on Au film coverage. For example, for Au/W(001) system,[27] the measured work function saturates at a value corresponding to the one of bulk Au at the least coverage of 3 ML Au.

Figure 4(c) presents topography (solid line) and ΔCPD (solid circles) profiles along the lines of the two 2D images, shown in Figs. 4(a) and 4(b). The profiles depict that the areas of increased ΔCPD correspond to the areas of the topographic features at their bases. The ΔCPD signal changes simultaneously with the topography one but the ΔCPD profile is steeper. The ΔCPD signal reaches its saturation levels in both uphill and downhill direction of the islands much faster than the topography signal. Since in KPFM, the topography image is due to the van der Waals and chemical interactions between the tip and the sample; with the relative contribution depending on the actual tip-apex shape, one can draw two conclusions. First, the observed changes of the ΔCPD signal faster than the topographic ones indicate that the Kelvin controller for surface potential compensation probes interactions, which have the interaction range shorter than that of the van der Waals. Second, the weak dependence of ΔCPD on the volume of imaged Au features indicates that the interaction is limited to the tip apex and the closest single surface gold atoms. These conclusions are further supported by the observed lack of dependence of ΔCPD on the Au island size [Fig. 4(d)]. As it is depicted in Fig. 4(d), the FM-KPFM measurements of the 2.0 nm thick Au islands of lateral edge sizes ranging from 8 up to 15 nm resulted in almost the same ΔCPD, whereas for the KBr/InSb system such a change of the KBr island size was reflected in a change of the ΔCPD by a factor of two (see Fig. 2).

E. Quasispectroscopic FM-KPFM measurements on Au/InSb(001) system

In order to evaluate the range of interaction contributing to the observed "high quality" of ΔCPD [like in Fig. 4(b)], we have performed "a quasispectroscopic" measurements for Au/InSb(001) system. We have found that for certain growth conditions on the InSb(001) surface, gold organizes itself in a form of flat and elongated islands (nanowires) of about 1 nm in height and few hundred nanometers in length.[28] This system, therefore, provides a good template for performing the required quasispectroscopic FM-KPFM measurements, as described below.

Using SPM technique at room temperature, it is usually difficult to perform reliable spectroscopy measurements over a specific surface site since the thermal drift and/or piezoscanner creep give large uncertainty, both for "in-plane" tip position as well as in its height determination. To overcome this problem, we have performed FM-KPFM measurements of the Au nanowires grown on InSb(001) surface in two distinct regimes of the imaging. In the first regime, we could acquire clear topography image of the Au islands with corresponding sharp CPD contrast, while in the other regime, the same Au islands can still be seen in the topography but can be hardly resolved in the corresponding CPD map. The former conditions correspond to imaging with relatively large detuning, in this case $\Delta f=-15$ Hz (tip "close" to the surface), whereas the latter ones correspond to imaging with a much smaller detuning of $\Delta f=-3$ Hz (the tip retracted from the surface). The system was stable and we could repeat this kind of imaging for several times. The imaging was performed with the fast scan direction being always perpendicular to the nanowire. Then, a sample surface with relatively low density of the islands has been chosen in such a way to have, in the AFM image frame, only a single Au nanowire. While imaging the nanowire after the acquisition of every few tens of scan lines, the detuning was gradually changed by 1 Hz between the two distinguished values of Δf, i.e., −15 and −3 Hz. The results are shown in Figs. 5(a) and 5(b) (topography and ΔCPD maps), respectively, with the corresponding scheme of the detuning magnitude changes. From the cross section of the topography image taken along the slow scan direction, the tip-surface separation changes have been extracted and attributed to the corresponding changes of the detuning. Whereas, from the cross sections taken along fast scan direction, the apparent island height with corresponding ΔCPD for a given detuning have been evaluated. Having calibrated the tip-surface distance change versus the detuning change, the dependences of the island height and the ΔCPD on the relative tip-surface separation change were obtained, as it is shown in Fig. 6. The zero value in the abscissa axis corresponds to the closest distance between the tip and the sample ($\Delta f=-15$ Hz). The decreasing of the detuning down to $\Delta f=-3$ Hz resulted in the increase of the tip-surface separation by 2.2 nm. The apparent island height exhibits slow decrease as the tip is retracted from the surface, whereas the ΔCPD exhibits a faster, exponential-like decay dependence on the tip-sample separation. The exponential fit $\Delta\text{CPD}\sim\exp(-\Delta z/\lambda)$ reveals the decay length of the ΔCPD signal of $\lambda=0.38$ nm. The faster disappearance of the ΔCPD signal than the topo-

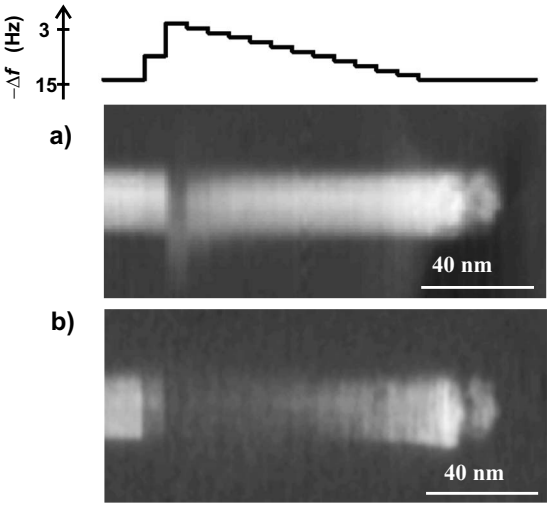

FIG. 5. (a) FM-KPFM topography and corresponding (b) ΔCPD map of Au island (nanowire) grown on InSb(001) surface at 560 K ($f_0=358,4$ kHz). The scheme shown over the image (a) reflects the changes of the detuning magnitude during acquisition of the images. For better visualization of the apparent change of the island height, the topography image was flatten with a line-by-line subtraction of an offset line in the fast scan direction.

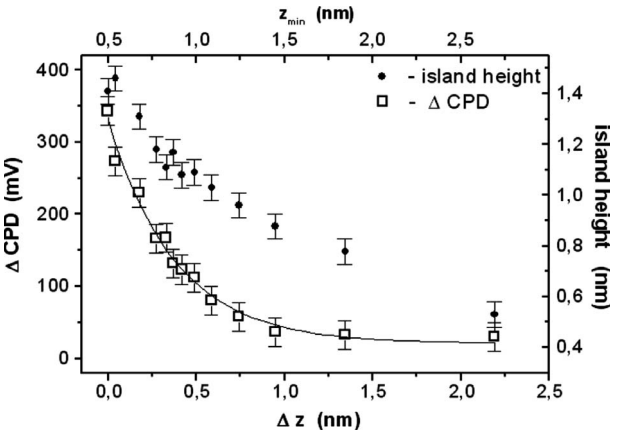

FIG. 6. Dependences of the apparent (a) Au island height and corresponding (b) ΔCPD on the tip-surface separation change. The upper abscissa axis, z_{min}, is the evaluated distance of the closest tip-surface approach (see in text).

graphic contrast as the tip is retracted from the surface indicates that the interactions contributing to the measured ΔCPD are of shorter range than the van der Waals ones. The observed saturation of ΔCPD signal on the level of about 30 mV at higher tip-surface separation is associated with the contribution of the true CPD due to the long-range electrostatic interactions between the tip and the Au island. We have evaluated the distance between the surface and the tip apex at its turning point (the closest approach) of the oscillation cycle, z_{min}, taking into account van der Waals interactions only. We have considered the following expression for the corresponding frequency shift derived for the van der Waals interaction between a sphere of radius R and infinite plane[18] $\Delta f_{vdW}/f_o = -HR/[12kAz_{min}(2z_{min}A)^{0.5}]$, where we used the experimental values of the cantilever spring constant $k=20$ N/m, the Hamaker constant[29] $H=8\times10^{-21}$ J, $R=20$ nm, and the vibration amplitude $A=20$ nm. From these data, we have evaluated the closest approach of the tip to the surface at the $\Delta f=-3$ Hz as $z_{min}=2.7$ nm (Fig. 6).

IV. DISCUSSION

The results presented in Sec. III C–III E provide the experimental evidence that in FM-KPFM technique, some short-range, bias-dependent interactions between the tip and the surface may be detected. These interactions eventually contribute to the observed "high quality" CPD contrast. A rough estimation of the tip-sample separation during the imaging of Au/InSb(001) system indicates that the interactions are detected when the tip-surface separation is of the order of 1 nm or smaller. For the tip being "far enough" from the surface, only long-range electrostatic interactions are bias dependent. In this case, FM-KPFM provides the CPD signal related to the surface potential distribution on the sample and the measured CPD contrast depends on the experimental conditions such as the ratio of the tip and surface structure dimensions. This is demonstrated for KBr/InSb(001) system where the measured CPD contrast depends on the KBr island size. This observation is then supported by the predictions of the theoretical model presented in this work, which takes into account only long-range electrostatic interactions between the tip and the surface.

When some other bias-dependent interactions between the tip and the surface are active, the interpretation of the experimental CPD contrast is more complicated. In this case, the measured CPD signal does not reflect the voltage that compensates the contact potential difference between the tip and the sample. Rather, it corresponds to the voltage for which the sum of the long-range electrostatic interaction (due to the contact potential difference between the tip and the sample) and the short-range interactions (related to the front tip atom and surface) has its minimum. In particular, the measured CPD signal does not reflect the distribution of the work function on the imaged surface.

There are some suggestions concerning the origin of the short-range and bias-dependent interactions. In the case of metal–metal interaction, Arai *et al.*[25] proposed that the increase of the attractive force in close tip-surface separation is due to a quantum-mechanical resonance. By changing the sample bias voltage, the Fermi level of the surface is tuned to that of the tip, resulting in the increase of the tunneling current and, finally, in the increase of strength of the total tip-sample interactions. Since during the imaging of the Au islands presented here, the tip can be contaminated with gold, this mechanism of increased bias-dependent metal–metal interactions cannot be excluded.

However, this is not the case for the imaging of clean InSb(001) surfaces, as it is shown in Fig. 3. For imaging of semiconductor surfaces, the covalent interactions between the front tip atom and the surface atoms are responsible for atomic contrast in topographic signal.[30] Thus, in the case of imaging of semiconductor surfaces, the origin of the CPD contrast on the atomic level most likely should be associated with the properties of covalent bonds. Here, we would like to give an intuitive explanation for the observed CPD contrast on the atomic scale. The image of the indium sublattice shown in Fig. 3(a) is due to the dominance of the covalent interaction between indium surface atoms and an antimony terminated tip.[13] Because the ionization energies of indium and antimony are different ($\Delta E_{ion.} = E^{Sb}_{ion.} - E^{In}_{ion.} = 2.84$ eV),[31] a polar covalent bond is formed between them, in which the sharing of the electron pair is unequal. An antimony, being more electronegative, is more negatively charged than indium. Thus, by changing the sample bias, one can influence In-Sb charge-transfer process and, finally, influence the strength (the binding energy) of their interaction. As the Kelvin controller minimizes the total tip-surface interaction with respect to the applied sample bias, the dark stripes in the CPD map [Fig. 3(b)] reflect lowering of the interaction when the lower potential is applied to the indium counterpart of the In-Sb interaction. The decrease of the sample voltage means that the In energy levels are tuned toward the energy levels of Sb atoms and, finally, induce that the covalent interaction between them gets less polar. The decrease of binding energy with decreasing of the molecular bond polarity is known and commonly observed. For example, for the hydrogen series, HF:HCl:HBr and HJ, the monotonic decrease of a percentage of ionic bonding in the total molecular binding from 45% for HF down to 5% for HJ molecule results in the

decrease of their binding energy from 5.80 to 3.05 eV for HF and HJ, respectively.[31] The simple picture of molecular interactions presented here qualitatively explains the observed feature of the CPD contrast resolution on the atomic scale range. In particular, it explains the observed inversion of the CPD signal with respect to the topographic one. However, the intuitive explanation needs to be proved by some theoretical calculations, which would include the charge redistribution in the tip-surface region.

V. SUMMARY AND CONCLUSIONS

In order to study the sensitivity and lateral resolution limits of KPFM technique, we have performed FM-KPFM imaging of bare semiconductor surfaces, as well as those covered with KBr and Au. We provide the experimental evidence that FM-KPFM is able to detect different bias-dependent interactions between the tip and the surface. The detection of multi bias-dependent interactions makes it difficult for the interpretation of the CPD contrast. In particular, when only the long-range electrostatic interactions are present due to the contact potential difference between the tip and the surface, the CPD signal reflect the work function distribution on the imaged surfaces. In this case, the CPD signal accuracy acquired with FM-KPFM depends on the tip and the surface structure dimensions, as it has been shown experimentally and theoretically. For the case of FM-KPFM imaging of KBr/InSb(001) system, we have found that the surface potential distribution can be acquired with lateral resolution of 3 nm. When some other short-range and bias-dependent interactions are detected, FM-KPFM provides even sub-nanometer resolution in the CPD contrast. In this case, however, the measured voltage is not related directly to the surface contact potential but reflects the behavior of the interactions between the tip front and the imaged surface atoms. Despite the problems with the distinction of the interactions contributing to the measured CPD signal, we have shown that FM-KPFM is a valuable tool that could provide the surface chemical sensitivity on the nanometer scale range. Both the KBr islands attached to the InSb(001) substrate terrace as well as gold spread over the flat InSb(001) surface could only be resolved because of the unique capabilities of FM-KPFM.

ACKNOWLEDGMENTS

This work was supported by the European Commission within the Integrated Project "Computing Inside Single Molecule Using Atomic Scale Technologies, Pico-Inside," Contract No. 015847 and Polish Ministry of Science and Higher Education (SPUB No. 249/6. PR UE/2006/7). The authors would like to thank J. J. Kolodziej for fruitful discussions.

*TEL: +48 12 6635632. FAX: +48 12 6337086. franciszek.krok@uj.edu.pl

[1] J. M. R. Weaver and D. W. Abraham, J. Vac. Sci. Technol. B **9**, 1559 (1991).
[2] M. Nonnenmacher, M. P. O'Boyle, and H. K. Wickramasinghe, Appl. Phys. Lett. **58**, 2921 (1991).
[3] M. M. Beerbom, B. Lagel, A. J. Cascio, B. V. Doran, and R. Schlaf, J. Electron Spectrosc. Relat. Phenom. **152**, 12 (2006).
[4] S. Sadewasser, Th. Glatzel, M. Rusu, A. Jager-Waldau, and M. Ch. Lux-Steiner, Appl. Phys. Lett. **80**, 2979 (2002).
[5] A. Schwarzman, E. Grunbaum, E. Strassburg, E. Lepkifker, A. Boa, Y. Rosenwaks, Th. Glatzel, Z. Barkay, M. Mazzer, and K. Barnham, J. Appl. Phys. **98**, 084310 (2005).
[6] T. Yamauchi, M. Tabuchi, and A. Nakamura, Appl. Phys. Lett. **84**, 3834 (2004).
[7] S. Sadewasser and M. Ch. Lux-Steiner, Phys. Rev. Lett. **91**, 266101 (2003).
[8] F. Krok, J. J. Kolodziej, B. Such, P. Czuba, P. Struski, P. Piatkowski, and M. Szymonski, Surf. Sci. **566-568**, 63 (2004).
[9] S. Kitamura, K. Suzuki, M. Iwatsuki, and C. B. Mooney, Appl. Surf. Sci. **157**, 222 (2000).
[10] K. Okamoto, Y. Sugawara, and S. Morita, Appl. Surf. Sci. **188**, 381 (2002).
[11] M. Goryl, F. Krok, J. J. Kolodziej, P. Piatkowski, B. Such, and M. Szymonski, Vacuum **74**, 223 (2004).
[12] M. Tomitori and T. Arai, Appl. Surf. Sci. **140**, 432 (1999).
[13] J. J. Kolodziej, B. Such, M. Szymonski, and F. Krok, Phys. Rev. Lett. **90**, 226101 (2003).
[14] For the simplicity of reading out of the experimental values, we define here the ΔCPD as a relative contrast of the CPD signal with respect to the lowest measured voltage, set as a zero, within the given CPD map.
[15] J. J. Kolodziej, B. Such, P. Czuba, F. Krok, P. Piatkowski, and M. Szymonski, Surf. Sci. **506**, 12 (2002).
[16] R. G. Jones, K. Singh, and C. F. McConville, Surf. Sci. **208**, L34 (1989).
[17] A. Sasahara, C. L. Pang, and H. Onishi, J. Phys. Chem. B **110**, 17584 (2006).
[18] M. Guggisberg, M. Bammerlin, Ch. Loppacher, O. Pfeiffer, A. Abdurixit, V. Barwich, R. Bennewitz, A. Baratoff, E. Meyer, and H.-J. Guntherodt, Phys. Rev. B **61**, 11151 (2000).
[19] Y. Rosenwaks, R. Shikler, Th. Glatzel, and S. Sadewasser, Phys. Rev. B **70**, 085320 (2004).
[20] U. Zerweck, Ch. Loppacher, T. Otto, S. Grafstrom, and L. M. Eng, Phys. Rev. B **71**, 125424 (2005).
[21] J. Konior, J. Appl. Phys. **101**, 084907 (2007).
[22] F. Giessibl, Rev. Mod. Phys. **75**, 949 (2003).
[23] B. Such, F. Krok, and M. Szymonski, in *Scanning Force Microscopies for Imaging and Characterisation of Nanostructured Materials in: Nanotechnology for Electronic Materials and Devices*, edited by A. Korkin, E. Gusev, J. K. Labanowski, and S. Luryi (Springer, Berlin, 2007).
[24] C. Kumpf, D. Smilgies, E. Landemark, M. Nielsen, R. Feidenhansl, O. Bunk, J. H. Zeysing, Y. Su, R. L. Johnson, L. Cao, J. Zegenhagen, B. O. Fimland, L. D. Marks, and D. Ellis, Phys. Rev. B **64**, 075307 (2001).
[25] T. Arai and M. Tomitori, Phys. Rev. Lett. **93**, 256101 (2004).

[26] M. Goryl, J. J. Kolodziej, F. Krok, P. Piatkowski, B. Such, and M. Szymonski, Microelectron. Eng. **81**, 394 (2005).
[27] G. W. Graham, Phys. Rev. B **32**, 2640 (1985).
[28] M. Szymonski, M. Goryl, F. Krok, J. J. Kolodziej, and F. Buatier de Mongeot, Nanotechnology **18**, 044016 (2007).
[29] L. Bergstrom, Adv. Colloid Interface Sci. **70**, 125 (1997).
[30] R. Perez, I. Stich, M. C. Payne, and K. Terakura, Phys. Rev. B **58**, 10835 (1998).
[31] *CRC Handbook of Chemistry and Physics*, edited by D. R. Lide (CRC, Boca Raton, 2001).